HHS Public Access

Author manuscript

J Am Chem Soc. Author manuscript; available in PMC 2022 January 13.

Published in final edited form as:

J Am Chem Soc. 2021 January 13; 143(1): 46–52. doi:10.1021/jacs.0c09688.

Temperature-Dependent Reactivity of a Non-heme $Fe^{III}(OH)(SR)$ Complex: Relevance to Isopenicillin N Synthase

Vishal Yadav,
Department of Chemistry, The Johns Hopkins University, Baltimore, Maryland 21218, United States

Maxime A. Siegler,
Department of Chemistry, The Johns Hopkins University, Baltimore, Maryland 21218, United States

David P. Goldberg*
Department of Chemistry, The Johns Hopkins University, Baltimore, Maryland 21218, United States

Abstract

Non-heme iron complexes with *cis*-$Fe^{III}(OH)(SAr/OAr)$ coordination were isolated and examined for their reactivity with a tertiary carbon radical. The sulfur-ligated complex shows a temperature dependence on ·OH versus ArS transfer, whereas the oxygen-ligated complex does not. These results provide the first working model for C−S bond formation in isopenicillin N synthase and indicate that kinetic control may be a key factor in the selectivity of non-heme iron "rebound" processes.

Isopenicillin N synthase (IPNS) belongs to a class of nonheme iron enzymes that utilize Fe^{II}/O_2 in the absence of a cosubstrate to catalyze the oxidation of L-Δ-(α-aminoadipoyl)-L-cysteinyl-D-valine (ACV) tripeptide to isopenicillin (IPN) (Scheme 1).[1−3] IPN gets further processed to form antibiotics such as penicillin and cephalosporins.[4−6] The biosynthesis of IPN is divided into two major steps: (a) formation of the β-lactam ring via $Fe^{III}–OO^{\bullet-}$ and Fe^{III}−OOH intermediates and (b) closure of the thiazolidine ring involving C−S bond formation from the reaction of a tertiary carbon radical (R·) with an $Fe^{III}(OH)(SR)$

*Corresponding Author David P. Goldberg −*Department of Chemistry, The Johns Hopkins University, Baltimore, Maryland 21218, United States*; dpg@jhu.edu.

ASSOCIATED CONTENT

Supporting Information

The Supporting Information is available free of charge at https://pubs.acs.org/doi/10.1021/jacs.0c09688.

X-ray crystallographic data for **1** (CIF)
X-ray crystallographic data for **2** (CIF)
X-ray crystallographic data for **3** (CIF)
X-ray crystallographic data for **4** (CIF)
X-ray crystallographic data for **6** (CIF)
X-ray crystallographic data for **5**·Li(OTf)(THF) (CIF)
Syntheses, ^1H and ^{19}F NMR spectra, Mössbauer data, UV−vis spectra, and computational details (PDF)

Complete contact information is available at: https://pubs.acs.org/10.1021/jacs.0c09688

The authors declare no competing financial interest.

intermediate.[7−11] Substrate probes have shown that other products besides the native thiazolidine compound can be formed (e.g., S-oxygenates,[10] thioacids,[12] and ring-expanded[13] or hydroxylated[14] products). These studies suggest that the substrate structure and orientation are important in determining the outcome of the reaction between R· and Fe^{III}(OH)(SR). Computational studies showed that sulfur transfer is kinetically favored over hydroxylation, supporting the observed selectivity of this step with the native substrate.[11,15] However, experimental studies that directly examine the C−S bond formation step are absent.

The inherent factors that may contribute to the selectivity of sulfuryl versus hydroxyl transfer in the absence of a protein pocket have not been examined previously. Similar selectivity arises for halogen versus hydroxyl transfer in the non-heme iron halogenases, and the properties that control the selectivity for halogenation are still under debate.[16−26] A few synthetic non-heme iron catalysts have shown some promise toward selective halogenation and related processes,[27−34] but the principles for designing a selective halogenation catalyst are not well-understood. Similarly, there are no reports describing the analogous Fe^{III}(OH)(SR) species, and no studies to date have shown selective sulfuryl over hydroxyl transfer mediated by a non-heme iron complex.

We previously developed a ligand with H-bonding groups ($BNPA^{Ph2}O^{-}$) that allowed us to isolate Fe^{III}(OH)(X) (X = OTf, Cl, Br) complexes and examine their reactivity toward carbon radicals.[35,36] Herein we report the first structurally characterized Fe^{III}(OH)(SAr) complex, prepared from $BNPA^{Ph2}O^{-}$, and describe its reactivity toward a tertiary carbon radical. The phenolate analogue, Fe^{III}(OH)(OAr), was also prepared and examined for comparative reactivity. A temperature-dependent switch in hydroxyl versus sulfur transfer is seen for the arylthiolate analogue.

Complexes $Fe^{II}(BNPA^{Ph2}O)(SPh^{p\text{-}NO2})$ (1) and $Fe^{II}(BNPA^{Ph2}O)(OPh^{p\text{-}NO2})$ (2) were synthesized by the addition of the appropriate sodium thiophenolate or phenolate salt to $Fe^{II}(BNPA^{Ph2}O)(OTf)$.[36] The crystal structures (Figure 1) revealed five-coordinate iron(II) complexes with the thiophenolate/phenolate ligand bound in place of OTf^{-}. Bond distances are typical for high-spin (hs) iron(II).[37−39]

The reactions of **1** and **2** with dry excess O_2 in THF at 23 °C (Scheme 2) led to the ferric complexes $Fe^{III}(BNPA^{Ph2}O)$- (OH)$(SPh^{p\text{-}NO2})$ (3) and $Fe^{III}(BNPA^{Ph2}O)(OH)(OPh^{p\text{-}NO2})$ (4), respectively, which were characterized by single-crystal X-ray diffraction (XRD). The crystal structures (Figure 2) reveal six-coordinate complexes with the thiophenolate or phenolate ligand bound in an equatorial position and a terminal hydroxide ligand occupying the axial H-bonded site, as observed previously.[35,36] The Fe^{III}−OH distances of 1.9034(18) and 1.908(2) Å in 3 and 4, respectively, are similar to those in other terminal Fe^{III}(OH) complexes.[38,40−48] In contrast, the Fe^{III}−S bond length of 2.4483(8) Å in 3 is longer than the few other non-heme high-spin Fe^{III}−SAr distances previously reported (2.35(1)−2.41(2) Å).[49−52] However, the analogous Fe^{III}−OAr distance of 2.000(3) Å in 4 is within the typical range (1.93−2.00 Å).[53−55]

Comparison of 3 and 4 shows that the phenolate group is trans to the alkoxide in 4, whereas the thiophenolate group is trans to a pyridine donor in 3. In addition, there is no $\pi-\pi$ stacking between the phenolate ring and any of the pyridine rings in 4, while there is $\pi-\pi$ stacking[56] between the thiophenolate group and the pyridine ring containing N(4) in 3. This interaction is characterized by a centroid-to-centroid distance of 3.6 Å and an angle of 9.3° between the least-squares planes of the two aromatic rings.[57]

A density functional theory (DFT) calculation gave Fe−S = 2.484 Å for 3, reproducing the elongated Fe−S bond length observed in the crystal structure. A comparison of the structure of 3 with an optimized geometry (QM/MM) for the proposed *cis*-Fe^{III}(OH)(SR) intermediate in IPNS[15] reveals a resemblance between the Fe^{III}–S and Fe^{III}–OH bond lengths of 2.37 and 1.87 Å, respectively, for IPNS, and those of 3. Thus, complex 3 is, to our knowledge, the first synthetic model of the proposed *cis*-Fe^{III}(OH)(SR) intermediate in IPNS.

The ^{1}H NMR spectra of 1 and 2 show relatively sharp paramagnetically shifted peaks from 90 to −10 ppm indicative of hs ($S = 2$) iron(II). In comparison, the spectra of 3 and 4 exhibit broad resonances from 80 to 10 ppm, as expected for a hs ($S = {}^5/_2$) Fe^{III} species. Zero-field Mössbauer spectroscopy of ^{57}Fe-enriched 1 and 2 shows sharp quadrupole doublets with parameters $\Delta = 0.94$ mm s^{-1} and $|\Delta E_Q| = 2.87$ mm s^{-1} for 1 and $\Delta = 1.03$ mm s^{-1} and $|\Delta E_Q| = 2.76$ mm s^{-1} for 2. Mössbauer analysis of ^{57}Fe-enriched 3 and 4 revealed broad quadrupole doublets with parameters $\Delta = 0.42$ mm s^{-1} and $|\Delta E_Q| = 0.96$ mm s^{-1} for 3 and $\Delta = 0.47$ mm s^{-1} and $|\Delta E_Q| = 1.01$ mm s^{-1} for 4. Such broadening for similar ferric complexes is known and can be explained by the population of an intermediate relaxation regime.[35,36,58,59]

The complex $Fe^{II}(BNPA^{Ph2}O)(OH)$ (5) was also prepared for comparison by adding OH^- to $Fe^{II}(BNPA^{Ph2}O)(OTf)$. Crystallization of 5 as orange blocks came from a reaction with LiOH and gave the structure shown in Figure 3. There is a lithium ion bound between OH^- and O1 and coordinated by OTf^- and THF, leading to the formula 5·Li(OTf)(THF). There is also an additional H-bond between OH^- and OTf^- that stabilizes the structure.

^{1}H NMR spectroscopy of 5 prepared in situ from ^{n}Bu$_4$NOH or from crystals of 5·Li(OTf)(THF) gave nearly identical spectra (Figures S9 and S10). Mössbauer spectroscopy on ^{57}Fe-5 synthesized from either ^{n}Bu$_4$NOH or LiOH in 2-MeTHF showed identical isomer shifts but different quadrupole splittings (Table S4). These trends for 5 versus the lithium adduct are reproduced by DFT calculations and support the coordination of Li^+ in solution.

The reaction of 3 with the substituted triphenylmethyl radical (p-OMe-C$_6$H$_4$)$_3$C· in toluene/THF at 23 °C was then examined. Triarylmethyl radicals are relatively stable and have been used recently by us and others to examine their reactivity with M−X (X = O, N, halide) bonds.[43,60−66,70] Analysis by ^{1}H NMR spectroscopy showed the complete conversion of the ferric complex 3 into the ferrous thiolate complex 1, consistent with selective hydroxyl transfer over sulfur transfer from the iron complex to the carbon radical (Scheme 3). The alcohol product (p-OMe-C$_6$H$_4$)$_3$COH was also identified in the ^{1}H NMR spectrum, and no evidence for formation of the thioether (p-OMe-C$_6$H$_4$)$_3$CSAr was

detected. Mössbauer spectroscopy provided additional corroborating data for the selectivity of ·OH transfer. The reaction of isotopically enriched ^{57}Fe-3 revealed a sharp quadrupole doublet with Δ = 0.96 mm s^{-1} and $|\Delta E_Q|$ = 2.83 mm s^{-1}, corresponding to the Fe^{II}(thiolate) complex 1 (Figure 4).

However, lowering the reaction temperature causes a dramatic shift in the product distribution. Addition of 1 equiv of (p-OMe-C_6H_4)$_3$C· to 3 at −35 °C for 1 h in THF/ toluene leads to the formation of Fe^{II}(OH) complex 5 instead of Fe^{II}(SPh$^{p\text{-}NO2}$) complex 1, as observed by ^{1}H NMR spectroscopy. Corresponding analysis by Mössbauer spectroscopy (Figure 4) reveals a sharp quadrupole doublet with Δ = 1.00 mm s^{-1} and $|\Delta E_Q|$ = 2.38 mm s^{-1}, which is a close match to the spectrum of 5. Taken together, the data show that sulfur transfer preferentially occurs over hydroxyl transfer at −35 °C (Scheme 3).

To examine the generality of these reactions, the p-CF_3-substituted complexes Fe^{II}(BNPA^{Ph2}O)(SAr$^{p\text{-}CF3}$) (6) and Fe^{III}(BNPA^{Ph2}O)(OH)(SAr$^{p\text{-}CF3}$) (7) were prepared (see the Supporting Information). Reaction of 7 with (p-OMe-C_6H_4)$_3$C· at −35 °C leads to formation of the Fe^{II}(OH) product 5, the same selectivity as seen for 3. The formation of (p-OMe-C_6H_4)$_3$CSPh$^{p\text{-}CF3}$ (80%) was also confirmed by ^{1}H NMR and ^{19}F NMR spectroscopy.

To examine the influence of temperature in more detail, the reaction of 3 and (p-OMe-C_6H_4)$_3$C· was carried out between 23 and −35 °C at intervals of 10 °C. The ^{1}H NMR spectrum for the reaction at 23 °C (Figure S45) shows only the presence of the Fe^{II}(SAr) complex, the product expected from selective · OH transfer. A second product begins to appear at −5 °C, as evidenced by new peaks at 84.8, 63.8, and 56.1 ppm. These peaks correspond to the Fe^{II}(OH) complex produced from ArS· transfer to the carbon radical. As the reaction temperature is further lowered, the ArS· transfer pathway becomes more favorable and is the dominant pathway by −25 °C. These data are consistent with a switch in mechanism that is dependent on the reaction temperature.

The phenoxide analogue Fe^{III}(OH)(OPh$^{p\text{-}NO2}$) (4) was reacted with the same tertiary carbon radical (p-OMe-C_6H_4)$_3$C· to examine the reactivity of an O donor versus an S donor. In contrast to the sulfur analogue, only ·OH transfer was seen by Mössbauer spectroscopy (Figure 5) and NMR spectroscopy at both 23 and −35 °C. The relative reaction rates of 3 and 4 with (p-OMe-C_6H_4)$_3$C· were assessed through competition experiments in which a 1:1 mixture of 3 and 4 was reacted with (p-OMe-C_6H_4)$_3$C· (1 equiv) at either 23 or −35 °C. The reaction at 23 °C led to the formation of only the Fe^{II}(OAr) product 2 along with unreacted 3, showing that · OH transfer is significantly faster from 4 than from 3.

However, reaction at −35 °C led to a small amount of (p-OMe-C_6H_4)$_3$C−SPh$^{p\text{-}NO2}$ (by TLC) and 5 (by ^{1}H NMR), together with the major product 2. These results show that ArS· transfer from 3 to the carbon radical has become competitive with ·OH transfer from 4 but still remains slower overall. We conclude that the relative rates of rebound follow the trend $k_{OH}(4) > k_{OH}(3)$ at 23 °C and $k_{OH}(4) > k_{SAr}(3)$ at −35 °C. The results from the reactions with (p-OMe-C_6H_4)$_3$C· are summarized in Scheme 4.

In summary, a new series of iron(II) and iron(III) complexes are described. The iron(III) complexes provide a platform to examine the competition between *cis*-ligated OH versus

SAr/OAr groups in reactions with carbon radicals. Reaction of Fe^{III}(OH)(SAr) with (p-OMe-$C_6H_4)_3C\cdot$ at 23 °C gives (p-OMe-$C_6H_4)_3$COH. However, the same reaction at −35 °C leads to the thioether (p-OMe-$C_6H_4)_3$CSAr. In contrast, Fe^{III}(OH)(OAr) produces only (p-OMe-$C_6H_4)_3$COH independent of temperature.

Transfer of ·OH from either 3 or 4 is likely thermodynamically favored because of the relative strength of the C−OH bond being formed, compared with the alternative C−OAr or C−SAr bonds.[67] Consistent with the expected thermodynamic trend in bond strengths, complexes 3 and 4 produce only (p-OMe-$C_6H_4)_3$COH at 23 °C. However, the same reaction for 3 at −35 °C preferentially produces (p-OMe-$C_6H_4)_3$CSAr. The equatorial Fe−S bond in 3 is significantly elongated and therefore weakened, resulting in a lower kinetic barrier for sulfur transfer.

The kinetic versus thermodynamic pathways are illustrated in the qualitative reaction coordinate diagram in Figure S46. This analysis implies that formation of the thioether is reversible at 23 °C, which is supported by the reductive cleavage of thioether bonds.[68,69] The Fe^{III}−OAr bond in 4, on the other hand, does not show any significant elongation, which is consistent with the lack of phenoxyl transfer.

Complex 3 is, to our knowledge, the first synthetic model of the ferric hydroxothiolate intermediate in IPNS. The overall reactivity of 3 is similar to that revealed by calculations on IPNS, which indicate that sulfur transfer is kinetically favored whereas hydroxylation is thermodynamically controlled.[15] These results show that the inherent electronic and structural features of a non-heme Fe center can significantly influence the outcome of the rebound step without contributions from an enzyme pocket or substrate orientation effects.

Supplementary Material

Refer to Web version on PubMed Central for supplementary material.

ACKNOWLEDGMENTS

The NIH (GM119374 to D.P.G.) is gratefully acknowledged for financial support. We thank Dr. Pierre LeMagueres (Rigaku Oxford Diffraction) for his help in obtaining the crystal structure of 4. Computer time was provided by the Maryland Advanced Research Computing Center (MARCC).

REFERENCES

(1). Roach PL; Clifton IJ; Hensgens CMH; Shibata N; Schofield CJ; Hajdu J; Baldwin JE Structure of isopenicillinN synthase complexed with substrate and the mechanism of penicillin formation. Nature 1997, 387, 827. [PubMed: 9194566]

(2). Cohen G; Shiffman D; Mevarech M; Aharonowitz Y. Microbial isopenicillin N synthase genes: structure, function, diversity and evolution. Trends Biotechnol. 1990, 8, 105. [PubMed: 1366527]

(3). Gordon JB; Goldberg DP Sulfur-Ligated, Oxidative Nonheme Iron Enzymes and Related Complexes. In Comprehensive Coordination Chemistry III; Liu Y, Que L, Eds.; Elsevier: London, 2020.

(4). Baldwin JE; Bradley M. Isopenicillin N synthase: mechanistic studies. Chem. Rev. 1990, 90, 1079.

(5). Blackburn JM; Sutherland JD; Baldwin JE A heuristic approach to the analysis of enzymic catalysis: Reaction of.delta.-(L-.alpha.-aminoadipoyl)-L-cysteinyl-D-.alpha.-aminobutyrate and.-

delta.-(L-.alpha.-aminoadipoyl)-L-cysteinyl-D-allylglycine catalyzed by isopenicillin N synthase isoenzymes. Biochemistry 1995, 34, 7548. [PubMed: 7779800]

(6). Baldwin JE; Abraham E. The biosynthesis of penicillins and cephalosporins. Nat. Prod. Rep. 1988, 5, 129. [PubMed: 3145474]

(7). Tamanaha E; Zhang B; Guo Y; Chang WC; Barr EW; Xing G; St. Clair J; Ye S; Neese F; Bollinger JM Jr.; Krebs C. Spectroscopic Evidence for the Two C-H-Cleaving Intermediates of Aspergillus nidulans Isopenicillin N Synthase. J. Am. Chem. Soc. 2016, 138, 8862. [PubMed: 27193226]

(8). Solomon EI; Brunold TC; Davis MI; Kemsley JN; Lee S-K; Lehnert N; Neese F; Skulan AJ; Yang Y-S; Zhou J. Geometric and Electronic Structure/Function Correlations in Non-Heme Iron Enzymes. Chem. Rev. 2000, 100, 235. [PubMed: 11749238]

(9). Roach PL; Clifton IJ; Fülöp V; Harlos K; Barton GJ; Hajdu J; Andersson I; Schofield CJ; Baldwin JE Crystal structure of isopenicillin N synthase is the first from a new structural family of enzymes. Nature 1995, 375, 700. [PubMed: 7791906]

(10). Burzlaff NI; Rutledge PJ; Clifton IJ; Hensgens CM; Pickford M; Adlington RM; Roach PL; Baldwin JE The reaction cycle of isopenicillin N synthase observed by X-ray diffraction. Nature 1999, 401, 721. [PubMed: 10537113]

(11). Lundberg M; Kawatsu T; Vreven T; Frisch MJ; Morokuma K. Transition States in a Protein Environment - ONIOM QM:MM Modeling of Isopenicillin N Synthesis. J. Chem. Theory Comput. 2009, 5, 222. [PubMed: 26609836]

(12). Ogle JM; Clifton IJ; Rutledge PJ; Elkins JM; Burzlaff NI; Adlington RM; Roach PL; Baldwin JE Alternative oxidation by isopenicillin N synthase observed by X-ray diffraction. Chem. Biol. 2001, 8, 1231. [PubMed: 11755401]

(13). Howard-Jones AR; Elkins JM; Clifton IJ; Roach PL; Adlington RM; Baldwin JE; Rutledge PJ Interactions of Isopenicillin N Synthase with Cyclopropyl-Containing Substrate Analogues Reveal New Mechanistic Insight. Biochemistry 2007, 46, 4755. [PubMed: 17397141]

(14). Daruzzaman A; Clifton IJ; Adlington RM; Baldwin JE; Rutledge PJ Unexpected Oxidation of a Depsipeptide Substrate Analogue in Crystalline Isopenicillin N Synthase. ChemBioChem 2006, 7, 351. [PubMed: 16444759]

(15). Lundberg M; Siegbahn PEM; Morokuma K. The Mechanism for Isopenicillin N Synthase from Density-Functional Modeling Highlights the Similarities with Other Enzymes in the 2-His-1-carboxylate Family. Biochemistry 2008, 47, 1031. [PubMed: 18163649]

(16). Srnec M; Solomon EI Frontier Molecular Orbital Contributions to Chlorination versus Hydroxylation Selectivity in the Non-Heme Iron Halogenase SyrB2. J. Am. Chem. Soc. 2017, 139, 2396. [PubMed: 28095695]

(17). Huang J; Li C; Wang B; Sharon DA; Wu W; Shaik S. Selective Chlorination of Substrates by the Halogenase SyrB2 Is Controlled by the Protein According to a Combined Quantum Mechanics/Molecular Mechanics and Molecular Dynamics Study. ACS Catal. 2016, 6, 2694.

(18). Quesne MG; de Visser SP Regioselectivity of substrate hydroxylation versus halogenation by a nonheme iron(IV)-oxo complex: possibility of rearrangement pathways. JBIC, J. Biol. Inorg. Chem. 2012, 17, 841. [PubMed: 22580819]

(19). Timmins A; Fowler NJ; Warwicker J; Straganz GD; de Visser SP Does Substrate Positioning Affect the Selectivity and Reactivity in the Hectochlorin Biosynthesis Halogenase? Front. Chem. 2018, 6, 513. [PubMed: 30425979]

(20). Timmins A; Quesne MG; Borowski T; de Visser SP Group Transfer to an Aliphatic Bond: A Biomimetic Study Inspired by Nonheme Iron Halogenases. ACS Catal. 2018, 8, 8685.

(21). Timmins A; de Visser SP A Comparative Review on the Catalytic Mechanism of Nonheme Iron Hydroxylases and Halogenases. Catalysts 2018, 8, 314.

(22). Mitchell AJ; Zhu Q; Maggiolo AO; Ananth NR; Hillwig ML; Liu X; Boal AK Structural basis for halogenation by iron- and 2-oxo-glutarate-dependent enzyme WelO5. Nat. Chem. Biol. 2016, 12, 636. [PubMed: 27348090]

(23). Matthews ML; Neumann CS; Miles LA; Grove TL; Booker SJ; Krebs C; Walsh CT; Bollinger JM Substrate positioning controls the partition between halogenation and hydroxylation in the aliphatic halogenase, SyrB2. Proc. Natl. Acad. Sci. U. S. A. 2009, 106, 17723. [PubMed: 19815524]

(24). Martinie RJ; Livada J; Chang W.-c.; Green MT; Krebs C; Bollinger JM; Silakov A. Experimental Correlation of Substrate Position with Reaction Outcome in the Aliphatic Halogenase, SyrB2. J. Am. Chem. Soc. 2015, 137, 6912. [PubMed: 25965587]

(25). Borowski T; Noack H; Radon M; Zych K; Siegbahn PEM Mechanism of Selective Halogenation by SyrB2: A Computational Study. J. Am. Chem. Soc. 2010, 132, 12887. [PubMed: 20738087]

(26). Pandian S; Vincent MA; Hillier IH; Burton NA Why does the enzyme SyrB2 chlorinate, but does not hydroxylate, saturated hydrocarbons? A density functional theory (DFT) study. Dalton Trans. 2009, 6201. [PubMed: 20449117]

(27). Puri M; Biswas AN; Fan R; Guo Y; Que L Jr. Modeling Non-Heme Iron Halogenases: High-Spin Oxoiron(IV)-Halide Complexes That Halogenate C-H Bonds. J. Am. Chem. Soc. 2016, 138, 2484. [PubMed: 26875530]

(28). Rana S; Biswas JP; Sen A; Clemancey M; Blondin G; Latour J-M; Rajaraman G; Maiti D. Selective C-H halogenation over hydroxylation by non-heme iron(iv)-oxo. Chem. Sci. 2018, 9 (40), 7843. [PubMed: 30429994]

(29). Chatterjee S; Paine TK Hydroxylation versus Halogenation of Aliphatic C-H Bonds by a Dioxygen-Derived Iron-Oxygen Oxidant: Functional Mimicking of Iron Halogenases. Angew. Chem., Int. Ed. 2016, 55, 7717.

(30). Comba P; Wunderlich S. Iron-Catalyzed Halogenation of Alkanes: Modeling of Nonheme Halogenases by Experiment and DFT Calculations. Chem. - Eur. J. 2010, 16, 7293. [PubMed: 20458709]

(31). Coin G; Patra R; Rana S; Biswas JP; Dubourdeaux P; Clemancey M; de Visser SP; Maiti D; Maldivi P; Latour J-M Fe-Catalyzed Aziridination Is Governed by the Electron Affinity of the Active Imido-Iron Species. ACS Catal. 2020, 10, 10010.

(32). Sasmal S; Rana S; Lahiri GK; Maiti D. Manganese-salen catalyzed oxidative benzylic chlorination. J. Chem. Sci. 2018, 130, 88.

(33). Rana S; Dey A; Maiti D. Mechanistic elucidation of C-H oxidation by electron rich non-heme iron(iv)-oxo at room temperature. Chem. Commun. 2015, 51, 14469.

(34). Rana S; Bag S; Patra T; Maiti D. Catalytic Electrophilic Halogenations and Haloalkoxylations by Non-Heme Iron Halides. Adv. Synth. Catal. 2014, 356, 2453.

(35). Yadav V; Rodriguez RJ; Siegler MA; Goldberg DP Determining the Inherent Selectivity for Carbon Radical Hydroxylation versus Halogenation with FeIII(OH)(X) Complexes: Relevance to the Rebound Step in Non-heme Iron Halogenases. J. Am. Chem. Soc. 2020, 142, 7259. [PubMed: 32281794]

(36). Yadav V; Gordon JB; Siegler MA; Goldberg DP Dioxygen-Derived Nonheme Mononuclear FeIII(OH) Complex and Its Reactivity with Carbon Radicals. J. Am. Chem. Soc. 2019, 141, 10148. [PubMed: 31244183]

(37). Gordon Z; Drummond MJ; Matson EM; Bogart JA; Schelter EJ; Lord RL; Fout AR Tuning the Fe(II/III) Redox Potential in Nonheme Fe(II)-Hydroxo Complexes through Primary and Secondary Coordination Sphere Modifications. Inorg. Chem. 2017, 56, 4852. [PubMed: 28394119]

(38). Cook SA; Ziller JW; Borovik AS Iron(II) Complexes Supported by Sulfonamido Tripodal Ligands: Endogenous versus Exogenous Substrate Oxidation. Inorg. Chem. 2014, 53, 11029. [PubMed: 25264932]

(39). MacBeth CE; Gupta R; Mitchell-Koch KR; Young VG; Lushington GH; Thompson WH; Hendrich MP; Borovik AS Utilization of Hydrogen Bonds To Stabilize M-O(H) Units: Synthesis and Properties of Monomeric Iron and Manganese Complexes with Terminal Oxo and Hydroxo Ligands. J. Am. Chem. Soc. 2004, 126, 2556. [PubMed: 14982465]

(40). Mukherjee J; Lucas RL; Zart MK; Powell DR; Day VW; Borovik AS Synthesis, Structure, and Physical Properties for a Series of Monomeric Iron(III) Hydroxo Complexes with Varying Hydrogen-Bond Networks. Inorg. Chem. 2008, 47, 5780. [PubMed: 18498155]

(41). MacBeth CE; Hammes BS; Young VG; Borovik AS Hydrogen-Bonding Cavities about Metal Ions: Synthesis, Structure, and Physical Properties for a Series of Monomeric M-OH Complexes Derived from Water. Inorg. Chem. 2001, 40, 4733.

(42). MacBeth CE; Golombek AP; Young VG; Yang C; Kuczera K; Hendrich MP; Borovik AS O2 Activation by Nonheme Iron Complexes: A Monomeric Fe(III)-Oxo Complex Derived From O_2. Science 2000, 289, 938. [PubMed: 10937994]

(43). Drummond MJ; Ford CL; Gray DL; Popescu CV; Fout AR Radical Rebound Hydroxylation Versus H-Atom Transfer in Non-Heme Iron(III)-Hydroxo Complexes: Reactivity and Structural Differentiation. J. Am. Chem. Soc. 2019, 141, 6639. [PubMed: 30969766]

(44). Gordon Z; Miller TJ; Leahy CA; Matson EM; Burgess M; Drummond MJ; Popescu CV; Smith CM; Lord RL; Rodríguez-Lopez J; Fout AR Characterization of Terminal Iron(III)-Oxo and Iron(III)-Hydroxo Complexes Derived from O_2 Activation. Inorg. Chem. 2019, 58, 15801. [PubMed: 31714068]

(45). Ford CL; Park YJ; Matson EM; Gordon Z; Fout AR A bioinspired iron catalyst for nitrate and perchlorate reduction. Science 2016, 354, 741. [PubMed: 27846604]

(46). Soo HS; Komor AC; Iavarone AT; Chang CJ A Hydrogen-Bond Facilitated Cycle for Oxygen Reduction by an Acidand Base-Compatible Iron Platform. Inorg. Chem. 2009, 48, 10024. [PubMed: 19780564]

(47). Ogo S; Yamahara R; Roach M; Suenobu T; Aki M; Ogura T; Kitagawa T; Masuda H; Fukuzumi S; Watanabe Y. Structural and Spectroscopic Features of a cis (Hydroxo)-FeIII-(Carboxylato) Configuration as an Active Site Model for Lipoxygenases. Inorg. Chem. 2002, 41, 5513. [PubMed: 12377047]

(48). Ogo S; Wada S; Watanabe Y; Iwase M; Wada A; Harata M; Jitsukawa K; Masuda H; Einaga H. Synthesis, Structure, and Spectroscopic Properties of [FeIII(tnpa)(OH)(PhCOO)]ClO4: A Model Complex for an Active Form of Soybean Lipoxygenase-1. Angew. Chem., Int. Ed. 1998, 37, 2102.

(49). Zhang S; Wang Q; Thierer LM; Weberg AB; Gau MR; Carroll PJ; Tomson NC Tuning Metal-Metal Interactions through Reversible Ligand Folding in a Series of Dinuclear Iron Complexes. Inorg. Chem. 2019, 58, 12234. [PubMed: 31448589]

(50). Li M; Bonnet D; Bill E; Neese F; Weyhermüller T; Blum N; Sellmann D; Wieghardt K. Tuning the Electronic Structure of Octahedral Iron Complexes [FeL(X)] (L = 1-Alkyl-4,7-bis(4-tert-butyl-2-mercaptobenzyl)-1,4,7-triazacyclononane, X = Cl, CH3O, CN, NO). The S = 1/2 ⇌ S = 3/2 Spin Equilibrium of [FeLPr(NO)]. Inorg. Chem. 2002, 41, 3444. [PubMed: 12079463]

(51). Noveron JC; Olmstead MM; Mascharak PK A Synthetic Analogue of the Active Site of Fe-Containing Nitrile Hydratase with Carboxamido N and Thiolato S as Donors: Synthesis, Structure, and Reactivities. J. Am. Chem. Soc. 2001, 123, 3247. [PubMed: 11457060]

(52). Gordon JB; Vilbert AC; DiMucci IM; MacMillan SN; Lancaster KM; Moenne-Loccoz P; Goldberg DP. Activation of Dioxygen by a Mononuclear Nonheme Iron Complex: Sequential Peroxo, Oxo, and Hydroxo Intermediates. J. Am. Chem. Soc. 2019, 141, 17533. [PubMed: 31647656]

(53). Bhowmik S; Dey S; Sahoo D; Rath SP Unusual Stabilization of an Intermediate Spin State of Iron upon the Axial Phenoxide Coordination of a Diiron(III)-Bisporphyrin: Effect of Heme-Heme Interactions. Chem. - Eur. J 2013, 19, 13732. [PubMed: 23999919]

(54). Velusamy M; Mayilmurugan R; Palaniandavar M. Iron(III) Complexes of Sterically Hindered Tetradentate Monophenolate Ligands as Functional Models for Catechol 1,2-Dioxygenases: The Role of Ligand Stereoelectronic Properties. Inorg. Chem. 2004, 43, 6284. [PubMed: 15446874]

(55). Hartley CL; DiRisio RJ; Chang TY; Zhang W; McNamara WR Electrocatalytic hydrogen evolution by an iron complex containing a nitro-functionalized polypyridyl ligand. Polyhedron 2016, 114, 133.

(56). Thakuria R; Nath NK; Saha BK The Nature and Applications of π-π Interactions: A Perspective. Cryst. Growth Des. 2019, 19, 523.

(57). Hunter CA; Sanders JKM The nature of HHH interactions. J. Am. Chem. Soc. 1990, 112, 5525.

(58). Mørup S. Magnetic Relaxation Phenomena. In Mössbauer Spectroscopy and Transition Metal Chemistry: Fundamentals and Applications; Gütlich P, Bill E, Trautwein AX, Eds.; Springer: Berlin, 2011; pp 201–234.

(59). Gupta R; Lacy DC; Bominaar EL; Borovik AS; Hendrich MP Electron Paramagnetic Resonance and Mössbauer Spectroscopy and Density Functional Theory Analysis of a High-Spin Fe^{IV}-Oxo Complex. J. Am. Chem. Soc. 2012, 134, 9775. [PubMed: 22574962]

(60). Zaragoza JPT; Yosca TH; Siegler MA; Moenne-Loccoz P; Green MT; Goldberg DP Direct Observation of Oxygen Rebound with an Iron-Hydroxide Complex. J. Am. Chem. Soc. 2017, 139, 13640. [PubMed: 28930448]

(61). Pangia TM; Yadav V; Gerard EF; Lin Y-T; de Visser SP; Jameson GNL; Goldberg DP Mechanistic Investigation of Oxygen Rebound in a Mononuclear Nonheme Iron Complex. Inorg. Chem. 2019, 58, 9557. [PubMed: 31313577]

(62). Pangia TM; Davies CG; Prendergast JR; Gordon JB; Siegler MA; Jameson GNL; Goldberg DP Observation of Radical Rebound in a Mononuclear Nonheme Iron Model Complex. J. Am. Chem. Soc. 2018, 140, 4191. [PubMed: 29537258]

(63). Jang ES; McMullin CL; Kaß M; Meyer K; Cundari TR¨; Warren TH Copper(II) Anilides in sp3 C-H Amination. J. Am. Chem. Soc. 2014, 136, 10930. [PubMed: 24940616]

(64). Lu X; Li X-X; Seo MS; Lee Y-M; Clémancey M; Maldivi P; Latour J-M; Sarangi R; Fukuzumi S; Nam W. A Mononuclear Nonheme Iron(IV)-Amido Complex Relevant for the Compound II Chemistry of Cytochrome P450. J. Am. Chem. Soc. 2019, 141, 80. [PubMed: 30558411]

(65). Iovan DA; Betley TA Characterization of Iron-Imido Species Relevant for N-Group Transfer Chemistry. J. Am. Chem. Soc. 2016, 138, 1983. [PubMed: 26788747]

(66). Bower JK; Cypcar AD; Henriquez B; Stieber SCE; Zhang S. C(sp3)-H Fluorination with a Copper(II)/(III) Redox Couple. J. Am. Chem. Soc. 2020, 142, 8514. [PubMed: 32275410]

(67). Blanksby SJ; Ellison GB Bond Dissociation Energies of Organic Molecules. Acc. Chem. Res. 2003, 36, 255. [PubMed: 12693923]

(68). Xiao J; Deng L. Synthesis, Structure, and Reactivity Study of Iron(II) Complexes with Bulky Bis(anilido)thioether Ligation. Organometallics 2012, 31, 428.

(69). Wang L; He W; Yu Z. Transition-metal mediated carbon-sulfur bond activation and transformations. Chem. Soc. Rev. 2013, 42, 599. [PubMed: 23079733]

(70). Cummins DC; Alvarado JG; Zaragoza JPT; Effendy Mubarak MQ; Lin Y-T; de Visser SP; Goldberg DP Inorg. Chem. 2020, 59, 16053. [PubMed: 33047596]

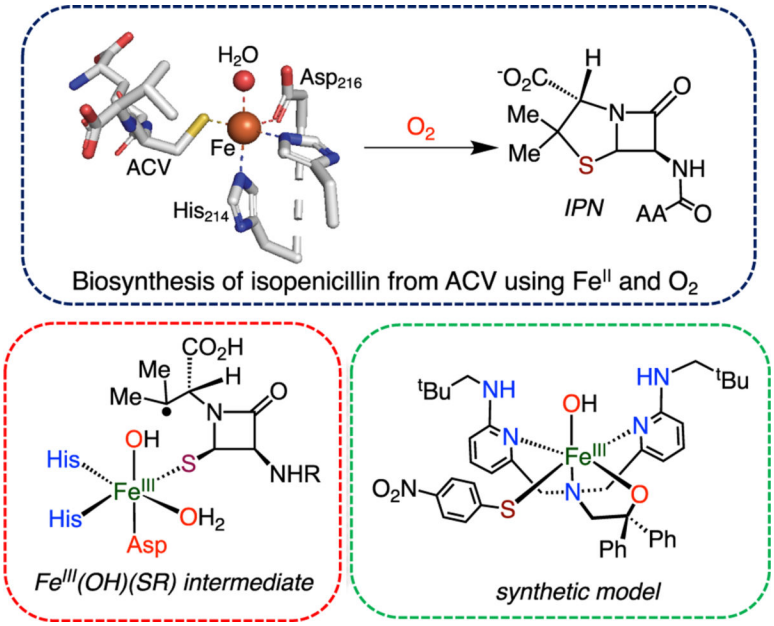

Scheme 1.
IPNS Reactivity and Model

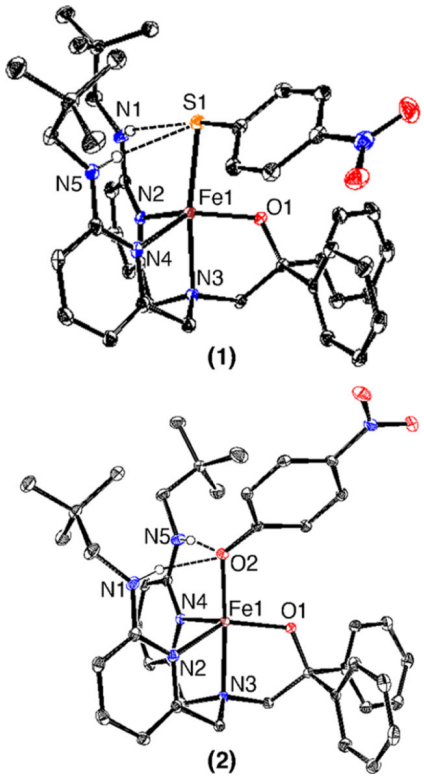

Figure 1.

Displacement ellipsoid plots (50% probability level) for 1 and 2 at 110(2) K. Hydrogen atoms (except for N−H) have been omitted for clarity.

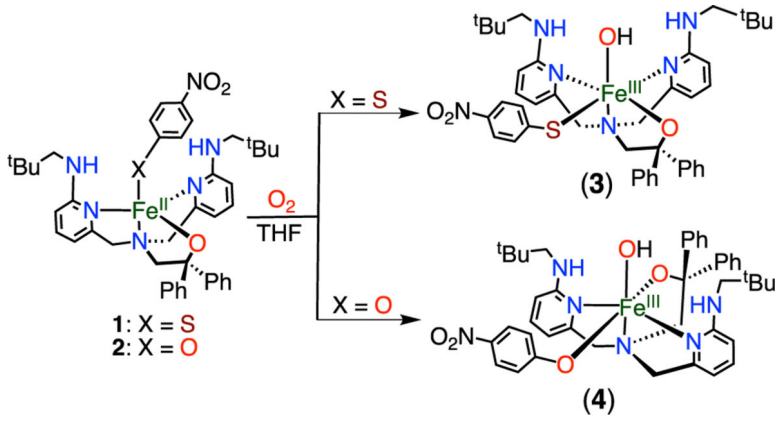

Scheme 2.
Synthesis of 3 and 4

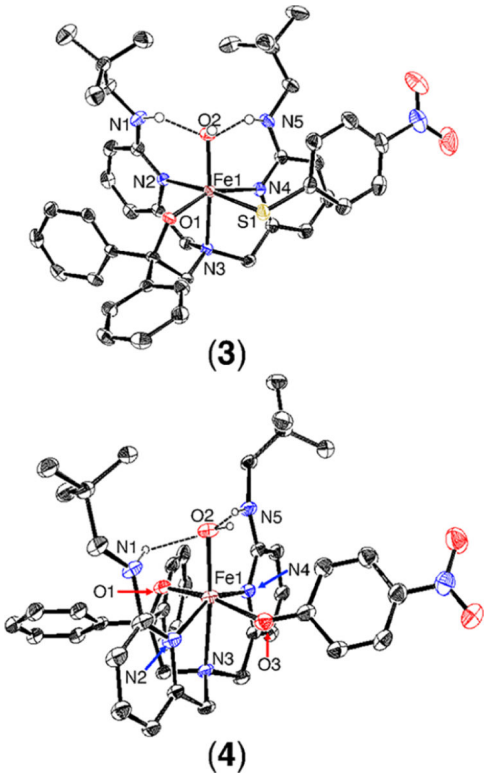

Figure 2.

Displacement ellipsoid plots (50% probability level) for 3 and 4 at 110(2) K. Hydrogen atoms (except for N−H and O−H) have been omitted for clarity.

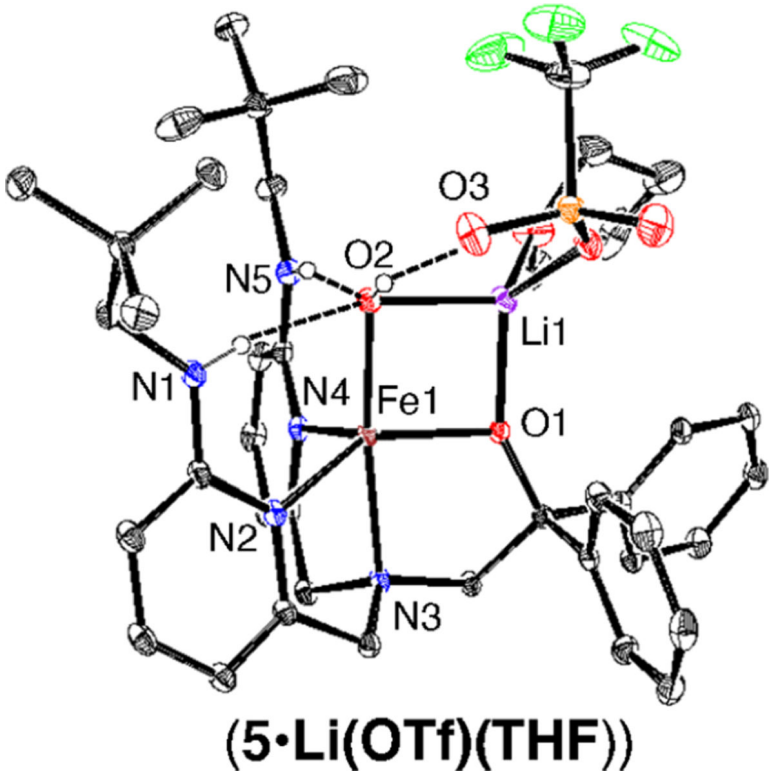

Figure 3.
Displacement ellipsoid plot (50% probability level) for 5· Li(OTf)(THF) at 110(2) K. Hydrogen atoms (except for N−H and O−H) are omitted for clarity.

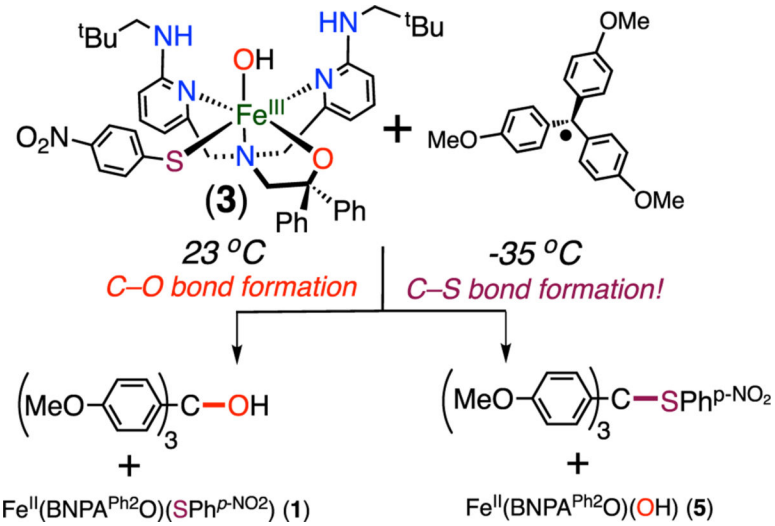

Scheme 3.
Reactions of 3 with Tertiary Carbon Radical

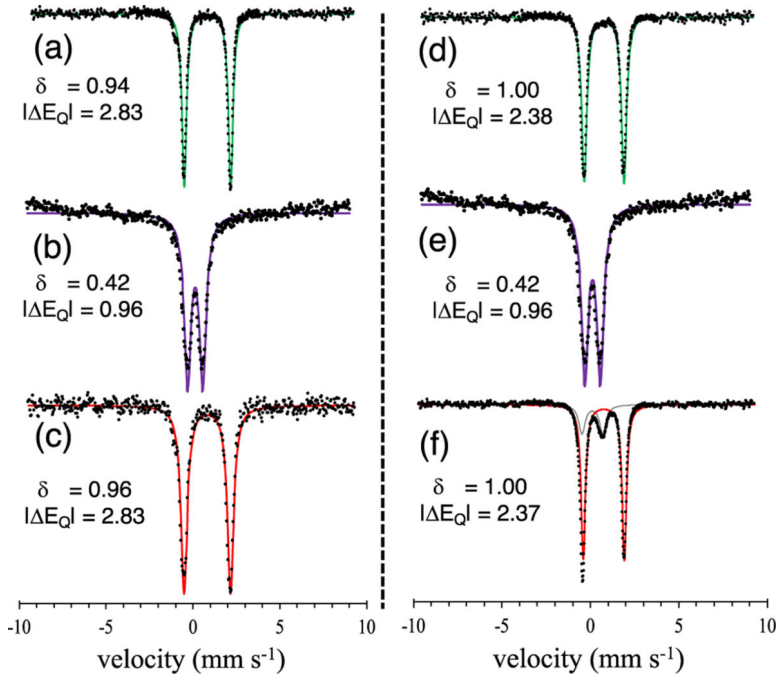

Figure 4.

Zero-field ^{57}Fe Mössbauer spectra (80 K) of (a) 1, (b) 3, and (c) 3 + (p-OMe-C_6H_4)$_3$C· at 23 °C and (d) 5, (e) 3, and (f) 3 + (p-OMe-C_6H_4)$_3$C· at −35 °C. Isomer shift (Δ) and quadrupole splitting (|ΔE_Q|) values are given in mm s^{-1}.

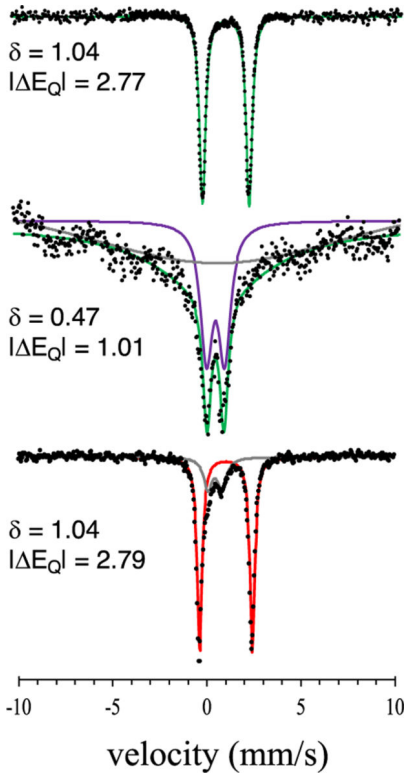

Figure 5.

Zero-field ^{57}Fe Mössbauer spectra (80 K) of (top) 2, (middle) 4, and (bottom) 4 + (*p*-OMe-$C_6H_4)_3C\cdot$ at 23 °C. Isomer shift (Δ) and quadrupole splitting ($|\Delta E_Q|$) values are given in mm s^{-1}.

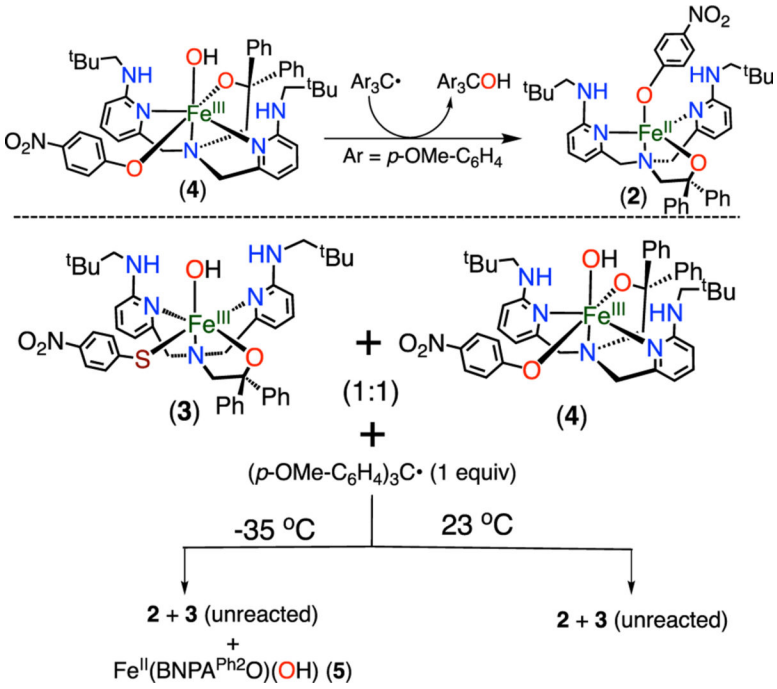

Scheme 4.
Reaction of 4 with Tertiary Carbon Radical